Photon-Assisted Tunneling through Self-Assembled InAs Quantum Dots in the Terahertz Frequency Range

K. Shibata,[1,2,*] A. Umeno,[1] K. M. Cha,[1] and K. Hirakawa[1,2,3,†]

[1]*Institute of Industrial Science, University of Tokyo, 4-6-1 Komaba, Meguro-ku, Tokyo 153-8505, Japan*

[2]*Institute for Nano Quantum Information Electronics, University of Tokyo, 4-6-1 Komaba, Meguro-ku, Tokyo 153-8505, Japan*

[3]*CREST-JST, 4-1-8 Honcho, Kawaguchi, Saitama 332-0012, Japan*

(Received 18 April 2012; published 16 August 2012)

We have investigated terahertz (THz) photon-assisted tunneling in single self-assembled InAs quantum dots (QDs). Two types of photon-assisted tunneling processes have been observed in the THz range: ground state resonance and photon-induced excited state resonance, depending on the relative magnitude between the orbital quantization energy of the QDs and the THz photon energy. Furthermore, we could realize a very high coupling efficiency between THz waves and QDs and observed multiphoton absorption up to the fourth-order during the tunneling process, resulting in almost complete lifting of the Coulomb blockade.

DOI: 10.1103/PhysRevLett.109.077401 PACS numbers: 78.67.Hc, 07.57.Kp, 73.40.Gk, 73.63.Kv

In a single electron transistor (SET), applying a time-varying oscillating potential to the Coulomb island can induce an inelastic tunneling event known as photon-assisted tunneling (PAT). PAT has been intensively studied in semiconductor SETs [1,2] in association with their device applications to quantum information processing [3,4]. These studies were performed in the GHz range and PAT in the terahertz (THz) range has only been studied for single wall carbon nanotubes [5].

Compared with the above mentioned SET systems, self-assembled InAs quantum dots (QDs) have the following unique properties: charging and orbital quantization energies are typically 10–40 meV [6,7], which corresponds to the THz range (2.5–10 THz). Moreover, electrons in InAs QDs have very large g factors and also experience strong spin-orbit interaction [8,9], which are important for the manipulation of electron spins in InAs QD systems. Particularly, it was reported recently that the spin-orbit interaction is electrically controllable [9] and also enables the spin-flip PAT [10], which removes existing restrictions for quantum control and detection of spins in the QDs through the PAT process. These properties of InAs QDs are attractive not only for their THz or spintronics device applications but also for investigations of carrier dynamics. Although a variety of the remarkable properties of InAs QD-SETs have already been revealed by observing artificial-atom properties [6,7], the Kondo effect [11], the superconducting proximity effect [12], and the spin valve properties [13], the THz response of InAs QDs has not been investigated yet and needs to be explored for electrical control of both carrier and spin dynamics in the THz range.

In this work, we have investigated electron transport through single self-assembled InAs QDs under THz wave irradiation. The fabricated QD samples operated as SETs in the few-electron regime, exhibiting clear shell structures. Under monochromatic THz irradiation, in addition to the original Coulomb oscillation peaks, new side peaks were observed, originating from the PAT of an electron in the QD to the electrodes. Moreover, we observed two types of PAT processes: ground state resonance and photon-induced excited state resonance, depending on the relative magnitude between the orbital quantization energy of the QDs and the THz photon energy. Furthermore, a very high coupling efficiency between the THz waves and the QDs was realized in our system, and multiphoton absorption was observed up to the fourth order during the tunneling process, resulting in an almost complete lifting of the Coulomb blockade.

The device structure is schematically shown in Fig. 1(a). Self-assembled InAs QDs were grown by molecular beam epitaxy on a (100)-oriented GaAs substrate. After successively growing a 300-nm-thick Si-doped GaAs layer, a 100-nm-thick $Al_{0.3}Ga_{0.7}As$ barrier layer, and a 200-nm-thick undoped GaAs buffer layer, self-assembled InAs QDs were grown at 480 °C. A pair of Ti (5 nm)/Au (15 nm) electrodes separated by a 20 nm gap was directly placed on an InAs QD and used as the source or drain electrodes, as shown in the inset of Fig. 1(b). A gate voltage V_G was applied to the Si-doped GaAs layer to change the number, N, of electrons in the QD. It is generally difficult to realize a strong interaction between THz radiation and electrons in nanometer-scale QDs due to their extremely small scattering cross sections. In order to improve the coupling efficiency between the THz waves and the electrons in the InAs QDs, a bow-tie antenna structure was implemented as the source-drain electrodes as shown in Fig. 1(b). Moreover, a hemispherical Si lens was placed on the back surface of the GaAs substrate, and the InAs QDs were illuminated with THz waves through the semi-insulating GaAs substrate [14]. THz radiation at frequencies, f_{THz}, ~2.5 THz, and 3.1 THz were generated by

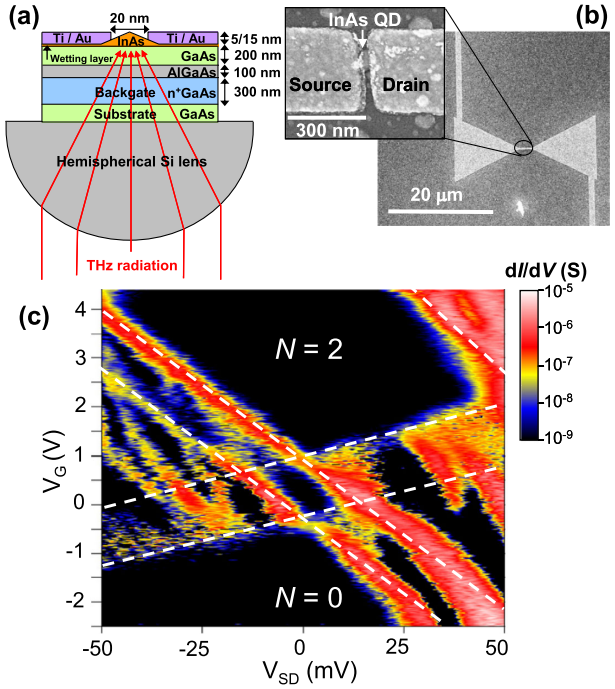

FIG. 1 (color online). (a) Schematic illustration of the device structure and the experimental setup. (b) An SEM image of a fabricated QD sample with a bow-tie antenna structure. The inset shows a SEM image of the nanogap metal electrodes bridged by a single InAs QD. (c) Coulomb stability diagram for a sample with a QD of $\sim 60 \times 60$ nm. The number of electrons, N, in each Coulomb diamond is also shown.

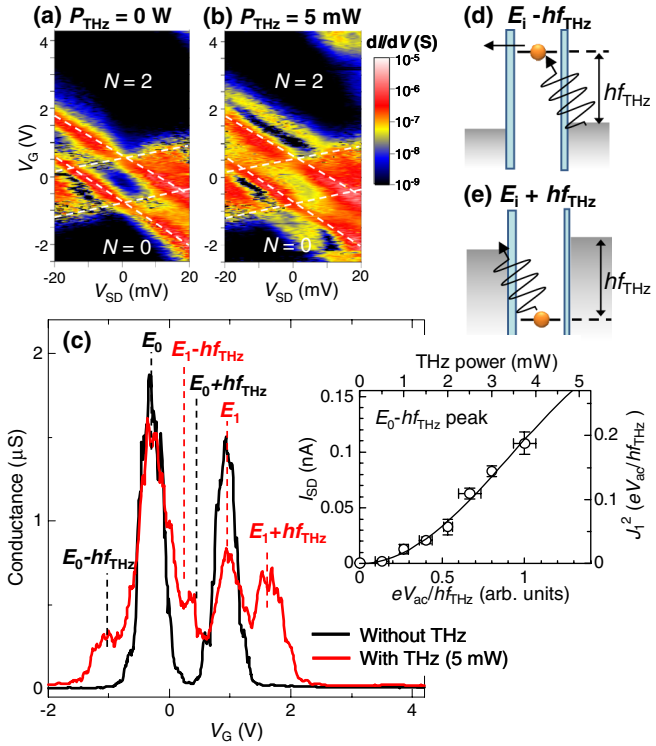

FIG. 2 (color online). (a) Coulomb stability diagram without THz irradiation. (b) Coulomb stability diagram under THz ($hf_{\mathrm{THz}} = 2.5$ THz, $P_{\mathrm{THz}} = 5$ mW) irradiation. (c) Linear conductance spectra as a function of V_{G} with (red line) and without (black line) THz irradiation. E_0 and E_1 denote the first and second occupied energy levels of the dot, respectively. The inset shows the dependence of the source-drain current, I_{SD}, at $V_{\mathrm{G}} = -1$ V (i.e., at E_0-hf_{THz}) on the THz power. Panels (d) and (e) show energy diagrams showing the sequence of tunneling events that dominantly contribute to the side peaks for different gate voltages, $E_i - hf_{\mathrm{THz}}$ and $E_i + hf_{\mathrm{THz}}$ ($i = 1, 2$), respectively. A small dc bias raises the right Fermi level with respect to the left Fermi level of the leads.

pumping methanol gas with a CO_2 laser. Fabricated samples were illuminated with the THz wave linearly polarized parallel to the long axis of the nanogap metal electrodes. The radiated THz power P_{THz} was measured just in front of the optical window of a ^{4}He cryostat; the actual THz radiation that reached the sample was much less. All the measurements were performed at 4.2 K.

Figure 1(c) shows the Coulomb stability diagram obtained by plotting the differential conductance dI/dV_{SD} as a function of the source-drain voltage V_{SD} and the backgate voltage V_G. Coulomb blockade takes place in the diamond shaped areas, each of which is associated with a well-defined number N of confined electrons in the QD. We can access a few-electron regime owing to the small lateral size of the QD ($\sim 60 \times 60$ nm) [7], and the Coulomb diamonds for $N = 1$ and 2 are clearly resolved [15]. From the difference in the addition energy for $N = 1$ and 2, the charging energy, E_C, and the orbital quantization energy difference between the s and p orbitals, $\Delta E_{s\text{-}p}$, were determined to be $E_C \sim 17$ meV and $\Delta E_{s\text{-}p} \sim 33$ meV, respectively.

Figures 2(a) and 2(b) show Coulomb stability diagrams without and with THz irradiation ($f_{\mathrm{THz}} = 2.5$ THz, $P_{\mathrm{THz}} = 5$ mW), respectively. Under THz irradiation, clear enhancement in the differential conductance appears as new lines parallel to the boundary of the Coulomb diamonds as shown in Fig. 2(b). In addition, the conductance also increases inside the $N = 1$ Coulomb diamond. These results clearly indicate that an additional tunneling channel opens due to the irradiation by THz waves. Figure 2(c) shows the linear response conductance spectra as a function of V_G with (red line) and without (black line) THz radiation. Without THz radiation, Coulomb oscillation peaks are observed. Under THz radiation, in addition to the original Coulomb peaks, new side peaks are clearly observed. It should be noted that the separation of the side peaks from the original Coulomb peaks corresponds exactly to the irradiated THz frequency ($hf_{\mathrm{THz}} = 10.3$ meV), as shown in Fig. 2(c), by using a conversion factor $\alpha \sim 0.015$ meV/mV, defined as the conversion ratio of V_G to energy. From these results, the side peaks are attributed to the PAT of electrons in the QD to the electrodes. Since $\Delta E_{s\text{-}p}(33\ \mathrm{meV}) > E_C(17\ \mathrm{meV}) > hf_{\mathrm{THz}}(10.3\ \mathrm{meV})$ in this QD sample, only the photon

sideband resonances of the ground state shown in Figs. 2(d) and 2(e) are observed. The inset of Fig. 2(c) shows the dependence of the PAT current at $V_G = -1$ V on the THz power. As the irradiated THz power increases, the current at the side peak increases. Theoretically, the tunneling rate into the 1-photon sidebands is expected to follow the square of the 1st-order Bessel functions of the radiation power, J_1^2. On the basis of this theory [16], the source-drain current I_{SD} is expressed as $I_{SD} = AJ_1^2(eV_{ac}/hf_{THz})$. Here, A is a conversion factor from the tunneling rate modulation into I_{SD}, e is the electron charge, and V_{ac} is an ac voltage induced in the QD by the THz electric field. Using this equation, we fit the data of the PAT current versus the THz power and display the results in the inset of Fig. 2(c) as a solid line. From this fit, we can roughly estimate the strength of the interaction between the electrons in the QD and the THz radiation. We found that $P_{THz} = 4$ mW at the optical window of the cryostat corresponds to $eV_{ac}/hf_{THz} \sim 1$ for this sample.

Figure 3(a) shows a Coulomb stability diagram for another QD sample with a lateral QD size of $\sim 70 \times 70$ nm. This sample also clearly exhibited Coulomb diamonds. Although the number of electrons in the QD could not be determined for this sample, we can tell the parity from the size of the Coulomb diamonds. From the size of the Coulomb diamonds, E_C and the orbital quantization energy difference ΔE were determined to be $E_C \sim 15$ meV and $\Delta E \sim 5$ meV, respectively, which lead to an energy relationship different from the previous sample, i.e., $E_C(15\text{ meV}) > hf_{THz}(10.3\text{ meV}) > \Delta E(5\text{ meV})$. Figure 3(b) shows the source-drain current I_{SD} as a function of V_G with (red curve) and without (black curve) THz irradiation of 1.5 mW. Current enhancement due to the THz irradiation is clearly observed under THz irradiation, except for the high V_G region [17]. In Fig. 3(b), we observed a clear current peak indicated by the blue arrow, which is not explained by the simple PAT process through the ground states shown in Figs. 2(d) and 2(e). The separation of this current peak from the original first Coulomb peak is $\Delta V_G \sim 0.37$ V. This V_G corresponds to an energy separation of ~ 5 meV, which is comparable to ΔE. These results strongly suggest that the current peak indicated by the blue arrow emerges because of the PAT of the electron in the ground state into the electrodes and subsequent tunneling of electrons from the leads through QD via the excited state, i.e., the photon-induced excited state resonance, as shown in Fig. 3(c). This tunneling process can be observed owing to the fact that ΔE is smaller than hf_{THz} in this particular sample [2].

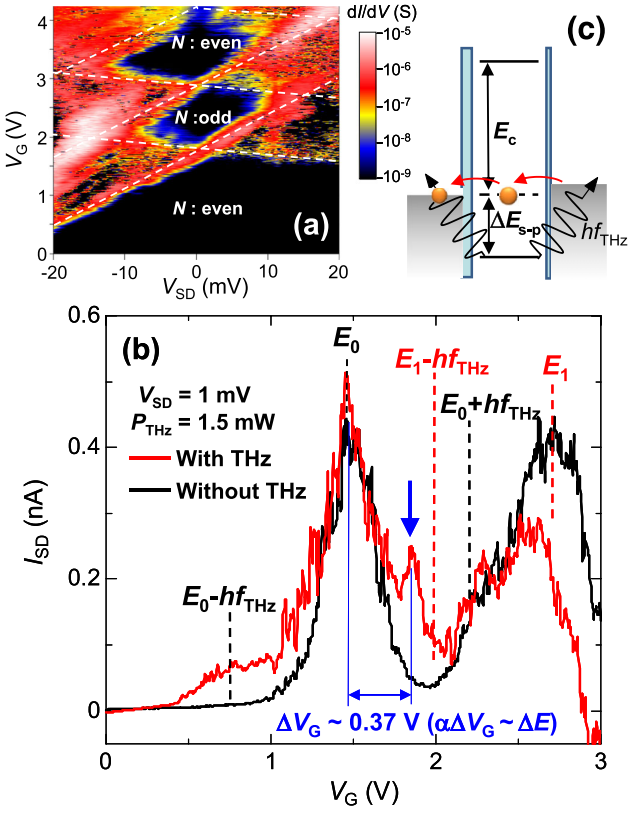

FIG. 3 (color online). (a) Coulomb stability diagram for a sample with a QD of $\sim 70 \times 70$ nm. (b) Source-drain current I_{SD} as a function of V_G at $V_{SD} = 1$ mV without (black) and with (red) THz wave irradiation ($hf_{THz} = 2.5$ THz, $P_{THz} = 1.5$ mW). (c) An energy diagram showing the sequence of the tunneling processes which contribute to the side peak shown by the blue arrow.

Figure 4(a) shows a Coulomb stability diagram for another QD sample with a lateral QD size of $\sim 40 \times 40$ nm. From the Coulomb diamonds, E_C and $\Delta E_{s\text{-}p}$ are determined to be $E_C \sim 35$ meV and $\Delta E_{s\text{-}p} \sim 45$ meV, respectively [15]. For this sample, the QD sample was carefully placed at the center of the hemispherical Si lens in order to improve the coupling efficiency between electrons in the QDs and the THz radiation. Figures 4(b) and 4(c) show Coulomb stability diagrams for $P_{THz} = 1$ and 5 mW, respectively. With increasing THz power, many satellite lines appear and the conductance of the sample steadily

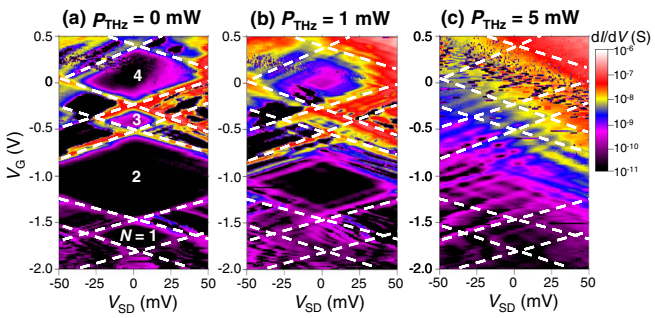

FIG. 4 (color online). Coulomb stability diagrams under THz irradiation (2.5 THz) for the THz power $P_{THz} = 0$ (a), 1 (b), and 5 mW (c), measured for a QD sample with a QD of $\sim 40 \times 40$ nm. The dashed lines are guides for the eye. The number of electrons in each Coulomb diamond is also shown.

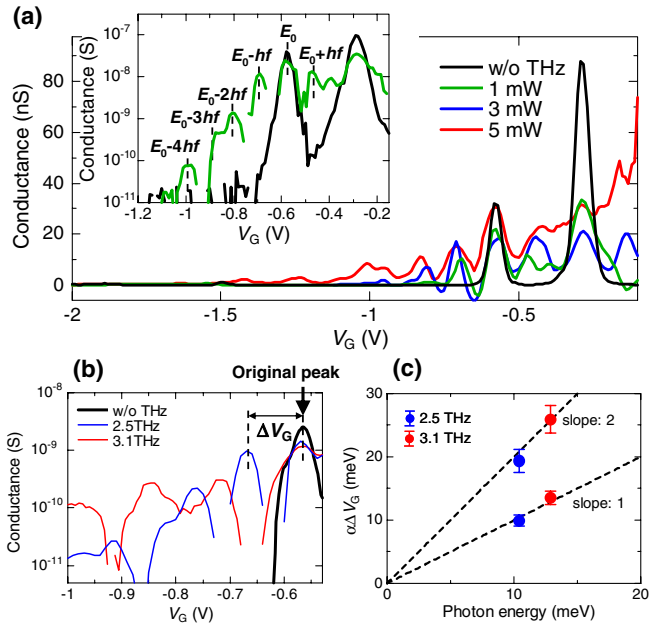

FIG. 5 (color online). (a) Linear conductance spectra as a function of V_G under several THz powers for $f_{\mathrm{THz}} = 2.5$ THz. The inset shows the linear conductance spectra for $P_{\mathrm{THz}} = 0$ and 1 mW on a logarithmic scale. (b) Linear conductance spectra for different THz frequencies of 2.5 and 3.1 THz. (c) The separation of the side peaks from the original Coulomb peak as a function of the photon energy of the THz wave plotted up to 2-photon absorption peaks. The dashed lines indicate $\alpha\Delta V_{\mathrm{G}} = hf_{\mathrm{THz}}$ and $\alpha\Delta V_{\mathrm{G}} = 2hf_{\mathrm{THz}}$.

increases, resulting in an almost complete lifting of the Coulomb blockade at $P_{\mathrm{THz}} = 5$ mW. This behavior strongly suggests that multiple photons are absorbed in this sample due to the high coupling efficiency between electrons in the QD and THz waves.

Figure 5(a) shows the linear conductances at several THz powers. The black curve shows the original Coulomb peaks measured without THz irradiation. As the THz power increases, side peaks appear corresponding to the absorption of multiple photons which are observed up to a photon number $n \sim 4$ at $P_{\mathrm{THz}} = 5$ mW. At high irradiation powers of ~5 mW, the THz irradiation strongly perturbs electron tunneling; this is a reflection of the nonlinear dependence of the peak heights on THz power, which is in agreement with the expected Bessel-function behaviors [16]. The inset of Fig. 5(a) shows the conductances as a function of V_G for $P_{\mathrm{THz}} = 0$ and 1 mW on a logarithmic scale. Even for P_{THz} as low as 1 mW, side peaks corresponding to the multiple phonon absorption are observed up to $n \sim 4$. In this figure, the conductance at 1-photon absorption peak is 1 order of magnitude higher than that at 2-photon absorption peak. From this result, it is roughly estimated that the $P_{\mathrm{THz}} = 1$ mW corresponds to $eV_{\mathrm{ac}}/hf_{\mathrm{THz}} \sim 1$, using the expected Bessel-function behavior; this means that the coupling efficiency is four-times higher than that for the previous sample. Finally, Fig. 5(b) shows the linear conductance as a function of V_G for the different THz frequencies of 2.5 and 3.1 THz. For both frequencies, side peaks are observed up to at least 2-photon absorption. It should be noted that the position of the side peaks changes, following the THz photon energy change. Figure 5(c) shows the separation of the side peaks from the original Coulomb peak as a function of the photon energy of the THz wave, plotted up to 2-photon absorption peaks. The data clearly show that the position of the side peaks depends linearly on the THz frequency, and that $\alpha\Delta V_G$ is in good agreement with $nhf_{\mathrm{THz}}(n = 1, 2)$. These results clearly indicate again that these side peaks are due to the THz PAT observed in self-assembled InAs QD systems. It should also be noted that these results are the first demonstration of a very high coupling efficiency between THz wave and electrons in QDs, which is sufficient for observing the multiphoton absorption.

In summary, we have investigated the electron transport through a single self-assembled InAs QD in a few-electron regime under THz wave irradiation. Under THz irradiation, new side peaks were observed, originating from the PAT of an electron in the QD to the electrodes. Moreover, we observed two types of PAT processes: ground state resonance and photon-induced excited state resonances, which depend on the relative magnitude between ΔE and hf_{THz}. Furthermore, we realized a very high coupling efficiency between the THz waves and the QDs and observed multiphoton absorption up to the fourth order during the tunneling process. These results are a clear demonstration of high coupling efficiency between THz radiation (wavelength ~100 μm) and electrons in nanometer-scale semiconductor QDs, which may open new possibilities of controlling carrier dynamics in quantum nanostructures by THz radiation.

We thank H. Sakaki and Y. Arakawa for continuous encouragement and S. Ishida for technical support. This work was partly supported by the Japan Science and Technology Corporation (CREST), Grants-in-Aid from the Japan Society for the Promotion of Science (No. 23681029 and No. 22241036), the research grants (the Murata Science foundation and the Research Foundation for Materials Science), and the Project for Developing Innovation Systems of MEXT.

*kshibata@iis.u-tokyo.ac.jp
†hirakawa@iis.u-tokyo.ac.jp

[1] L. P. Kouwenhoven, S. Jauhar, J. Orenstein, P. L. McEuen, Y. Nagamune, J. Motohisa, and H. Sakaki, Phys. Rev. Lett. **73**, 3443 (1994).
[2] T. H. Oosterkamp, L. P. Kouwenhoven, A. E. A. Koolen, N. C. van der Vaart, and C. J. P. M. Harmans, Phys. Rev. Lett. **78**, 1536 (1997).
[3] J. R. Petta, A. C. Johnson, J. M. Taylor, E. A. Laird, A. Yacoby, M. D. Lukin, C. M. Marcus, M. P. Hanson, and A. C. Gossard, Science **309**, 2180 (2005).

[4] F. H. L. Koppens, C. Buizert, K. J. Tielrooij, I. T. Vink, K. C. Nowack, T. Meunier, L. P. Kouwenhoven, and L. M. K. Vandersypen, Nature (London) **442**, 766 (2006).

[5] T. Fuse, Y. Kawano, T. Yamaguchi, Y. Aoyagi, and K. Ishibashi, Nanotechnology **18**, 044001 (2007); Y. Kawano, T. Fuse, S. Toyokawa, T. Uchida, and K. Ishibashi, J. Appl. Phys. **103**, 034307 (2008).

[6] M. Jung, T. Machida, K. Hirakawa, S. Komiyama, T. Nakaoka, S. Ishida, and Y. Arakawa, Appl. Phys. Lett. **87**, 203109 (2005).

[7] K. Shibata, M. Jung, K. M. Cha, M. Sotome, and K. Hirakawa, Appl. Phys. Lett. **94**, 162107 (2009).

[8] S. Takahashi, R. S. Deacon, K. Yoshida, A. Oiwa, K. Shibata, K. Hirakawa, Y. Tokura, and S. Tarucha, Phys. Rev. Lett. **104**, 246801 (2010).

[9] Y. Kanai, R. S. Deacon, S. Takahashi, A. Oiwa, K. Yoshida, K. Shibata, K. Hirakawa, Y. Tokura, and S. Tarucha, Nature Nanotech. **6**, 511 (2011).

[10] L. R. Schreiber, F. R. Braakman, T. Meunier, V. Calado, J. Danon, J. M. Taylor, W. Wegscheider, and L. M. K. Vandersypen, Nature Commun. **2**, 556 (2011).

[11] Y. Igarashi, M. Jung, M. Yamamoto, A. Oiwa, T. Machida, K. Hirakawa, and S. Tarucha, Phys. Rev. B **76**, 081303(R) (2007); K. Shibata and K. Hirakawa, Appl. Phys. Lett., **93**, 062101 (2008).

[12] Y. Kanai, R. S. Deacon, A. Oiwa, K. Yoshida, K. Shibata, K. Hirakawa, and S. Tarucha, Phys. Rev. B **82**, 054512 (2010).

[13] K. Hamaya, M. Kitabatake, K. Shibata, M. Jung, M. Kawamura, K. Hirakawa, T. Machida, T. Taniyama, S. Ishida, and Y. Arakawa, Appl. Phys. Lett. **91**, 022107 (2007).

[14] B. J. Keay, S. J. Allen, Jr., J. Galán, J. P. Kaminski, K. L. Campman, A. C. Gossard, U. Bhattacharya, and M. J. W. Rodwell, Phys. Rev. Lett. **75**, 4098 (1995).

[15] The number of electron in each Coulomb diamond was determined (1) from the parity dependence of the size of Coulomb diamonds and (2) from the relationship between the size of the QDs and the expected orbital quantization energy difference between the s and p orbitals, $\Delta E_{s\text{-}p}$, as determined in Ref. [7].

[16] P. K. Tien and J. R. Gordon, Phys. Rev. **129**, 647 (1963).

[17] The current suppression at high V_G region under THz irradiation is probably due to the lower frequency ac voltage components superimposed to the applied dc V_{SD}.